

Calibration of ultrasonic sensors using optoacoustics.

Amir Rosenthal, Vasilis Ntziachristos, and Daniel Razansky

Institute for Biological and Medical Imaging, & Chair for Biological Imaging Technische Universität of München and Helmholtz Zentrum München, Ingolstädter Landstraße 1, 85764 Neuherberg, Germany

ABSTRACT

Ultrasonic detectors are commonly calibrated by finding their response to incident plane waves. However, in optoacoustics, the response to broadband point sources is required. To induce such sources using the optoacoustic effect, the illuminated object's dimensions must be smaller than the resolution achievable by the optoacoustic system. The main difficulty in such measurements is that the magnitude of the field emitted by such sources is proportional to their dimensions, and thus may be weak compared to parasitic sources in the setup. In this work we experimentally demonstrate two methods for calibrating acoustic detectors. In both methods, acoustic sources are optoacoustically induced in large optically absorbing slabs. Despite the large dimensions of the illuminated objects, the geometry used yields wide-band acoustic fields, which are perceived by the detectors as originating from point sources.

Keywords: optoacoustics, photoacoustics, acoustic sensors, acoustic calibration.

1. INTRODUCTION

Most popular piezoelectric ultrasonic detectors attain relatively limited bandwidth and non-uniform frequency characteristics, leading to distortion of the detected acoustic signals. In imaging applications, signal distortions are translated into image artifacts and loss of accuracy. Such artifacts can be reduced if the detector characteristics which are relevant to the imaging modality are known and corrected for. Thus, the calibration of ultrasonic detectors is not only important for assessing image fidelity, but may also be used for improving the overall quantification abilities.

Several calibration methods have been developed using acoustic plane waves¹⁻⁶. One of the early methods employed was the reciprocity method in which the same transducer or transducers is used both as the source and as the detector¹⁻³. Using this technique, the efficiency of the transducer in both modes is embodied in the measured acoustic signal. The known relation between these two efficiencies, manifested in the reciprocity parameter, is then utilized to extract both of them from the measurement. One of the advantages of the reciprocity method is that it does not require using a primary standard, i.e. an acoustic detector whose response is known. A different approach which avoids using a primary standard is to measure the driving voltage fed into a transducer and use a modeling approach to calculate the formed acoustic field⁴. The calibration is performed by placing a hydrophone in front of the transducer and comparing its measured signal to the one predicted by the model. When a primary standard is used, the calibration of acoustic detectors is performed by creating a wide-band acoustic field, and measuring it with both the primary standard and the sensor that is to be calibrated. By comparing the two detected signals, the frequency response of the detector can be calculated. The acoustic fields can be created by wide-band transducers^{5,6}, or by nonlinear acoustic propagation effects⁷. The primary standard may be a pre-calibrated hydrophone⁷ or a setup based on optical interferometry^{6,7}.

In recent years there has been a growing interest in new imaging modalities based on the thermoacoustic effect, which require calibrated acoustic sensors in order to perform quantified imaging⁸⁻¹². In optoacoustic tomography, for instance, ultra-wideband acoustic fields are generated by thermal expansion of tissue exposed to high-power short laser pulses. Here, the imaged object acts as an acoustic (or optoacoustic) source. Since the detection is acoustic, optoacoustic tomography is capable of mapping optical contrast while attaining diffraction-limited ultrasonic resolution, not affected by light diffusion. Furthermore, techniques like multispectral optoacoustic tomography (MSOT), in which the laser

operates at multiple wavelengths, extend this mapping capability to imaging and mapping bio-distribution of spectrally-distinct molecular biomarkers, attracting a great deal of interest also from the biological and medical communities¹²⁻¹⁴. Optoacoustic imaging typically operates with much wider band signals as compared to conventional ultrasound imaging; therefore the detector characterization needs to operate over wider frequency bands in order to attain accurate image quantification.

One of the common detection geometries in optoacoustic tomography is based on focused transducers that are cylindrically focused in the detection plane⁹⁻¹¹. Owing to their large detection area, the use of focused sensors significantly improves the signal-to-noise ratio of the measurement, which is a limiting factor in optoacoustic tomography. However, the use of such detectors introduces a difficulty since their sensitivity should be measured for a point source in their focal plane¹², and not for a plane wave. If the plane-wave sensitivity is measured instead, the large size of the detector will suppress high-frequency components, which would be readily detectable if an optoacoustic point source were placed in the imaged plane. Thus, the vast majority of existing acoustic calibration techniques cannot be easily adapted in optoacoustic tomography.

A preferable way of calibrating acoustic sensors in optoacoustic setups is to use the optoacoustic effect itself to generate wide-band acoustic fields. The generated fields are characterized by measurements with a primary standard¹⁵, or assumed to have a uniform spectrum in the frequency band of interest^{16,17}. The acoustic sources can, for instance, be created by illuminating a large area of highly absorbing substance^{15,17}. Due to the high absorption, light cannot penetrate deep in the medium, leading to energy deposition mostly on the surface of the absorbing medium, which in turn yields wideband acoustic fields. However, owing to the large area of illumination, the created sources are approximately planar rather than point sources. Thus, such a technique is mostly suitable for calibrating small area unfocused acoustic detectors.

In Ref. [16] the calibration was alternatively performed by directly illuminating a spherically focused acoustic detector with ultra-short nanosecond-duration flashes of light. Since the entire surface of the transducer was illuminated simultaneously, it was assumed that the measured response effectively emulates the response to a point source with a uniform spectrum located in the focal region of the transducer. While this method produces a wideband acoustic field, it involves several limiting factors which may lead to substantial inaccuracies. First, the acoustic sources follow different patterns of diffraction, reflection, and refractions, since they were created within the detector, whereas the desired calibration needs to be due to fields originating outside the transducer surface. Second, the method ignores pyroelectric effects that may induce parasitic electric currents within the detector. Third, the field created in such an experiment does not have a uniform spectrum. Because of the inherent bipolar nature of optoacoustic fields, their spectral content usually approaches zero near the DC frequencies rather than being constant. While this property is well known and crucial for spectral calibrations, it has not been widely considered so far in technical papers^{16,17}.

In order to induce wideband point acoustic sources using the optoacoustic effect, the illuminated object's dimensions must be considerably smaller than the resolution achievable by the optoacoustic system. The main difficulty in such measurements is that the amplitude of the field emitted by such sources is proportional to their dimensions, and thus may be weak compared to other parasitic optoacoustic sources in the setup. This difficulty is particularly challenging in the low-frequency regime, where the field from such sources is even weaker. The tradeoff between the amplitude of the generated acoustic fields and the corresponding spectral width is one of the limiting factors that have prevented the use of this approach for characterizing optoacoustic detectors.

In this paper we consider and experimentally demonstrate two novel methods developed for calibrating acoustic detectors using optoacoustics. In both methods, optoacoustic sources are induced in relatively large optically absorbing slabs by illuminating them with short laser pulses. Although the large dimensions of the illuminated objects would normally lead to narrowband acoustic fields, the specific geometry used yields wideband fields, which are perceived by the detectors as originating from point sources. The two methods were experimentally tested by measuring the frequency response of a cylindrically focused transducer to sources in the focal region. Despite the inherent difference between the

two methods, the obtained frequency responses were almost identical. The results of the two methods were further cross-validated by measuring the transducer's response to microspheres positioned in the focal plane and illuminated by short laser pulses, which constituted true wideband point sources. A very good match was obtained across most of the frequency span between the frequency responses obtained using the microspheres and using two methods developed in this paper. The frequency responses showed large differences only in the low-frequency regions, in which the signal generated by the microspheres was not sufficiently strong.

2. THEORETICAL ANALYSIS

In an acoustically homogenous medium, under the condition of thermal confinement⁸, the optoacoustically induced pressure wave $p(r,t)$ obeys the following equation¹⁸:

$$\frac{\partial^2 p(r,t)}{\partial t^2} - v^2 \nabla^2 p(r,t) = \Gamma H_r \frac{\partial H_t(t)}{\partial t} \quad (1)$$

where v and ρ are velocity of sound in tissue and its density, Γ is the Grüneisen parameter, and $H(r,t) = H_r(r)H_t(t)$ is the amount of energy absorbed in the tissue per unit volume and per unit time, which is the source for the acoustic fields. In the case in which $H_t(t) = \delta(t)$, there is an analytical solution to Eq. 1. which is given by a Poisson-type integral¹⁸

$$p_\delta(r,t) = \frac{\Gamma}{4\pi v} \frac{\partial}{\partial t} \int_{R=vt} \frac{H_r(r')}{R} dA', \quad (2)$$

where $R = |r - r'|$ while the integration is performed over a sphere with a radius of $R = vt$. The pressure wave for a general temporal profile $H_t(t)$ is obtained by convolving $p_\delta(r,t)$ in Eq. 2 with $H_t(t)$. The acoustic signal measured by a point detector with an impulse response $h(t)$ at r is thus

$$p(r,t) = p_\delta(r,t) * h(t) * H_t(t), \quad (3)$$

where $*$ denotes the convolution operation. When the calibration of the system is performed for optoacoustic applications, one wishes to extract $h(t) * H_t(t)$ out of $p(r,t)$. When the absolute sensitivity of the acoustic sensor alone is desired, $H_t(t)$ should be deconvolved out of Eq. 3, or alternatively, be sufficiently short to be approximated by a delta function. Since typical laser pulses used in optoacoustic measurements have an ultra-short duration of few nanoseconds to tens of nanoseconds, $H_t(t)$ can be substituted by a delta function if the frequencies of interest are considerably lower than 100MHz.

In order to extract $h(t) * H_t(t)$ out of $p(r,t)$, the function $p_\delta(r,t)$ should be known and have a bandwidth larger than that of $h(t) * H_t(t)$. Generally, the bandwidth of an optoacoustic signal is inversely proportional to the axial dimension of the source, as seen from the position of the detector. This heuristic property is generally valid for approximately uniform optoacoustic sources with smooth boundaries and similar dimensions on both axial and lateral axes. An example of such a source is a uniformly illuminated absorbing sphere¹⁶. The properties of such sources are depicted in Figs. 1a-1c. In Fig. 1a, the point detector is shown in red, whereas the optoacoustic source $H_r(r)$ is shown in gray. Assuming $H_r(r)$ is equal to 1 within the gray area and zero outside it, the integral in Eq. 2 will have similar

attributes to the curve shown in Fig. 1b, and the spectrum of $p_{\delta}(r,t)$ will have the attributes of the curve in Fig. 1c. According to Fig. 1c, in order to obtain high amplitudes at high frequency, the object should be wide in the lateral dimension a and short in the axial dimension b . However, this heuristic approach is mostly true for round objects with similar axial and lateral dimensions, i.e. $a \approx b$. In other cases, the lateral dimension might also affect the bandwidth of the optoacoustic signal.

For studying the effect of the lateral dimension on the properties of the optoacoustic signal, we analyze the signal created by a rectangular optoacoustic source. The geometry of the source and the detector is shown in Fig 1d, where $b, c \gg a$. In this geometry, most of the acoustic field arrives from the proximal and distal edges of the rectangular. The reason for this is that the integral in Eq. 2 is slowly varying for arcs within the rectangle and changes rapidly only when they intersect the proximal or distal edge. The duration of the signal generated at the proximal edge is equal to the difference between the maximal and minimal distances from the sensor to points on the edge divided by the speed of sound. For $a \ll c$ this duration is given by

$$\Delta t = \frac{a^2}{8c\nu} \tag{4}$$

Assuming b is large enough to ignore the signal from the distal edge, the bandwidth in this geometry will be inversely proportional to Δt and will not be a function of b . In this case, the duration of the entire signal will be given by the expression in Eq. 4 and will not be proportional to any of the dimensions in the geometry. The effective length of the proximal edge as seen by the detector is $a/(8c)$ times smaller than the lateral dimension of the edge. The bandwidth of the signal is increased by the same factor when compared to the geometry in Fig. 1a. This property can be used to create strong wide-bandwidth optoacoustic sources and is the basis of our calibration method.

In order to justify the geometrical analysis, we solve Eq. 2 analytically for the geometry given in Fig 1d:

$$p_{\delta}(r,t) = \frac{\Gamma}{2\pi(\nu t)^2} \begin{cases} 0 & \nu t < c \\ p_1(r,t) & c \leq \nu t < \sqrt{c^2 + \left(\frac{a}{2}\right)^2} \\ p_2(r,t) & \sqrt{c^2 + \left(\frac{a}{2}\right)^2} \leq \nu t < b \\ p_3(r,t) & b \leq \nu t < \sqrt{(c+b)^2 + \left(\frac{a}{2}\right)^2} \\ 0 & \sqrt{(c+b)^2 + \left(\frac{a}{2}\right)^2} \leq \nu t \end{cases} \tag{5a}$$

where

$$\begin{aligned}
p_1(r,t) &= \frac{1}{\sqrt{\left(\frac{vt}{c}\right)^2 - 1}} - \cos^{-1}\left(\frac{c}{vt}\right); \\
p_2(r,t) &= -\frac{1}{\sqrt{\left(\frac{2vt}{a}\right)^2 - 1}} - \sin^{-1}\left(\frac{a}{2vt}\right); \\
p_3(r,t) &= -\frac{1}{\sqrt{\left(\frac{2vt}{a}\right)^2 - 1}} - \sin^{-1}\left(\frac{a}{2vt}\right) - \frac{1}{\sqrt{\left(\frac{vt}{c+b}\right)^2 - 1}} + \cos^{-1}\left(\frac{c+b}{vt}\right)
\end{aligned} \tag{5b}$$

The function $p_1(r,t)$ in Eqs. 5a and 5b corresponds to the field generated by the proximal edge of the rectangular source; $p_2(r,t)$ corresponds to the field from the bulk; and $p_3(r,t)$ corresponds to the field from the distal edge. Equations 5a and 5b show that the acoustic field is infinite for $t=c/v$. This result does not create any contradictions in the model because the excitation is described by a delta function, which is infinite too. For $a \ll c$, it can be readily seen that the signal from the proximal edge has the time duration given in Eq. 4. In addition, if we compare the minimal signal from the proximal edge to the maximum signal from the bulk, both obtained around $t = \sqrt{c^2 + (a/2)^2} / v$, we find that the quotient of the two signals is approximately equal to $2(c/a)^2 \gg 1$. Thus, neglecting the signal originating from the bulk is justified.

The geometrical approach can also be applied to finite size detectors. Similarly to the case of a point detector, the duration of the optoacoustic signal is equal to the maximum and minimum distances between the detector and the source's edge divided by the speed of sound. In this case, the distances are calculated by finding a point on the detector and a point on the source edge whose distance is maximal or minimal compared to any other set of two points. In the case of a flat detector, shown in Fig. 1e, the signal time duration is given by

$$\Delta t = \frac{(a+d)^2}{8cv} \tag{6}$$

Eq. 6 shows that our geometry is also useful for finite-size detectors. When $d \ll a$, the signal's duration is similar to that of a point detector. When $a \ll d$, the duration increases considerably, but is still comparable to the duration that would be obtained for a point source ($a=0$). Thus, in this case, the rectangular source effectively emulates a point source. For $a \approx d$, the increase in the signal's duration might require reducing the size of the edge to better simulate an impulse point source. Nonetheless, the signal duration would still be considerably smaller than a/v .

The last geometry studied in this paper is of the curved detector shown in Fig. 1f. The focus of the detector is on the middle of the proximal edge of the source. The duration of the optoacoustic signal for this geometry is given by

$$\Delta t = \begin{cases} \frac{(a+d)^2}{8cv} & d < a \\ \frac{ad}{2cv} & d \geq a \end{cases} \tag{7}$$

For the cases of $d \ll a$ and $a \approx d$, the duration is similar to that of a flat detector, and results in a signal duration significantly smaller than a/v . However, for $a \ll d \approx c$, the duration is comparable to a/v , thus offering no significant advantage over standard geometries.

The short duration of the signal from the proximal edge is used in both our calibration methods. In both methods, it is required that this duration be sufficiently short to approximate an impulse function. Under this condition, the measured response from the proximal edge is approximately equal to the impulse response of the detector. In method I, the value of b fulfills $b > T/v$, where T is the duration of the detector's impulse response and v is the speed of sound in the medium. This choice yields a temporal separation between the responses of the two edges, which allows us to use temporal windowing to extract the impulse response and thus the frequency response. In method II, we choose $b \ll c$. In that case, the response of the distal edge is approximately equal to the opposite of the response from the proximal edge. Thus, if the proximal-edge field emulates a point impulse source, and b is sufficiently small, the entire source will emulate a point derivative-impulse source. As a result, the response measured by the detector will be the derivative of its impulse response. The frequency response of the detector can be found from such a measurement by integrating the measured acoustic fields and performing the Fourier transform.

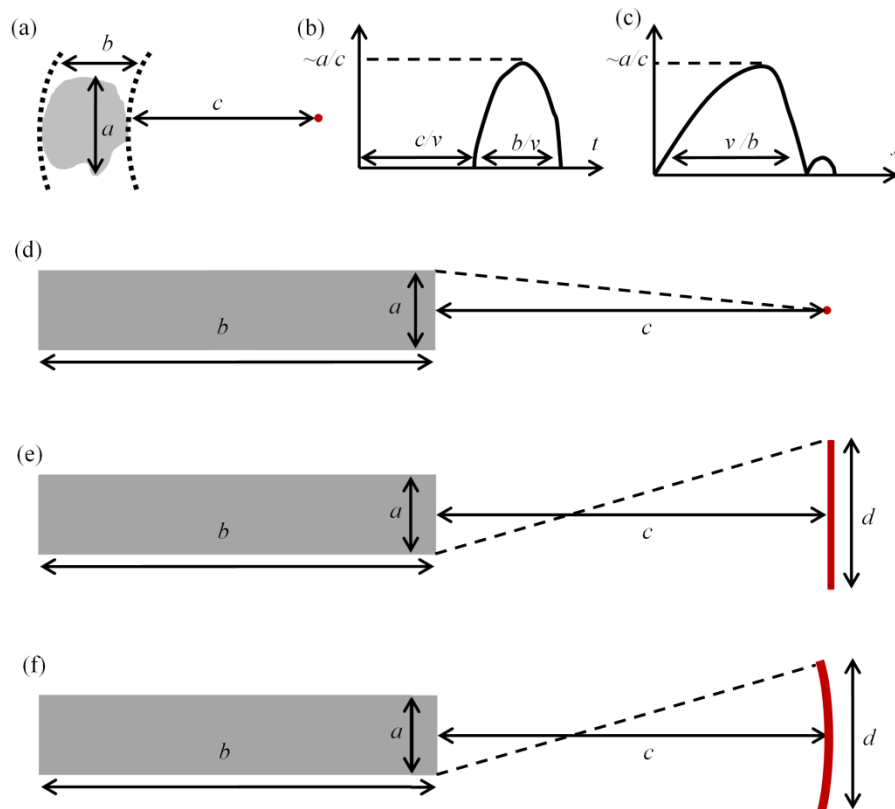


Fig.1 A scheme of the different 2D configurations analyzed in this paper for measuring the frequency response of acoustic detectors. The acoustic sources are equal to one in the gray areas and to zero outside them; the detectors are marked in red. (a) A source with a smooth boundary and similar dimensions on the axial and lateral axes and a point detector. The dashed curves represent the two extreme arcs over which the integral in Eq. 2 is nonzero. (b) A heuristic description of the integral in Eq. 2 and of (c) the spectrum of $p_s(r,t)$ for the geometry in Fig. 1a. (d-e) A rectangular optoacoustic source with point, flat, and curved detectors, respectively. The curved detector is focused on to the middle of the proximal edge of the source. The curved lines represent the longest distances from any point on the detectors to any point on the proximal edge of the sources.

3. EXPERIMENTAL METHODS AND RESULTS

In this section we demonstrate the performance of the two calibration methods considered for measuring the frequency response of a common piezoelectric transducer cylindrically-focused in the detection plane (Model V382, Panametrics, Olympus NDT, Waltam, MA). The results were compared to the frequency responses obtained by illuminating microspheres positioned in the focal plane and by directly illuminating the transducer. The transducer was round-shaped with a diameter of 1.3 cm, which was cylindrically focused with a focal length of 38 mm. The optoacoustic setup was similar to one used in Ref. [19]. Briefly a tunable OPO laser (MOPO-710, Spectra-Physics, Mountain View, CA, USA), providing <8 nsec duration pulses with 30 Hz repetition frequency in the visible spectrum (450–680 nm), was used in order to illuminate optically absorbing phantoms in order to create optoacoustic sources. In all our experiments, we used a 650 nm wavelength at an average output laser power of approximately 800 mW. The acoustic transducer was positioned to focus onto a plane parallel to the optical table.

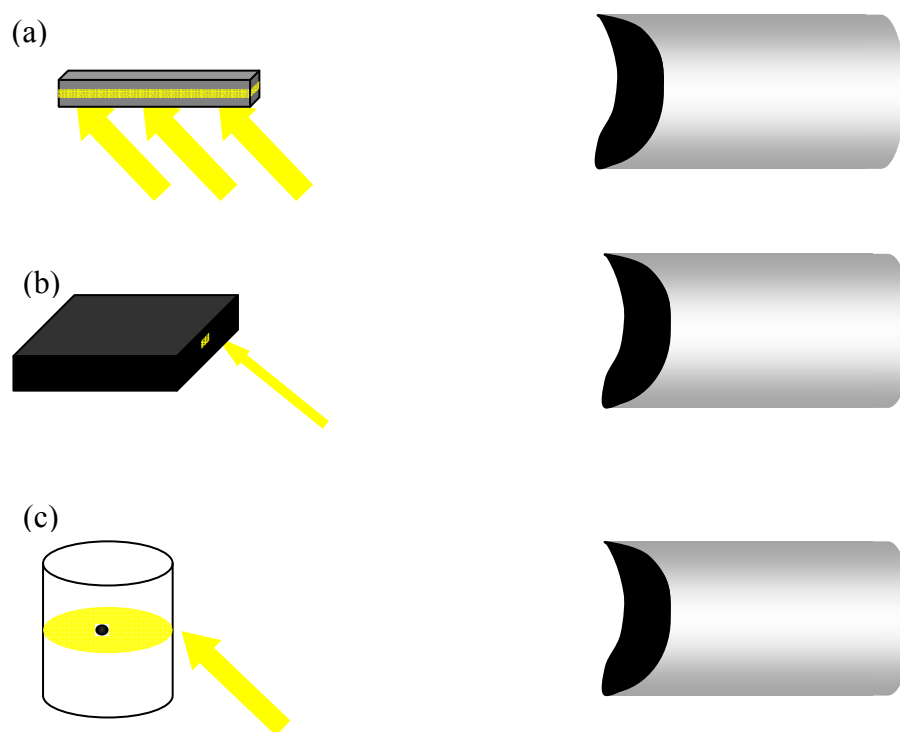


Fig.2. A schematic description of the different geometries used to measure the frequency response of the acoustic detector. The yellow arrows denote the illumination, whereas the dark parts signify absorbing elements.

3.1 Method I ($b > T/v$)

In the first experiment, we used a slab phantom to emulate a point-impulse acoustic source according to method I. The phantom was prepared by mixing 1.3% (by weight) of agar powder and 0.09% (by volume) of black India ink (Higgins, Sanford Bellwood, IL) in water heated to 96 deg and pouring the solution into a slab mold. After solidification, the obtained slab phantoms had an absorption coefficient of $\mu_a = 0.1 \text{ cm}^{-1}$ and the following dimensions: 30mm x 2mm x 2mm. For this absorption coefficient, the light attenuation within the phantom was insignificant, resulting in a uniform optoacoustic source. The phantom was positioned with its proximal face located in the focal plane of the transducer at a distance of approximately 38 mm. Figure 2a shows the geometry of the experiment, where the illuminated part of the

phantom is shown yellow. In order to provide a uniform optoacoustic source, we used engineered diffusers to broaden and homogenize the laser beam in the detection plane. In addition, the beam was passed through a horizontal slit to create a light sheet and limit its width to 0.5 mm, effectively creating a slab source with a 2mm x 0.5mm face. According to our numerical simulation this source effectively emulates a point-impulse source over a bandwidth of 20 MHz.

The impulse response of the detector was obtained by windowing the measured signal to include the response to only the proximal edge. Figure 3a shows the obtained impulse response (solid-blue curve). The impulse response was Fourier transformed to obtain the frequency response, whose amplitude and phase are shown in Fig 3b and 3c. Figure 3d shows the amplitude of the impulse response in log scale.

3.2 Method II ($b \ll c$)

In the second experiment, we used a highly absorbing slab phantom to emulate a point impulse-derivative acoustic source according to method II. The phantom was prepared by mixing approximately 0.13mg of agar powder with 10ml of black India ink heated to 96 deg and pouring the solution into a slab mold. The resulting phantom had an absorption coefficient of approximately $\mu_a = 110 \text{ mm}^{-1}$ and the following dimensions: 30mm x 30mm x 2mm. The phantom was positioned 4 cm from the transducer as shown in Fig. 2b. The laser beam was passed through horizontal and vertical slits with widths of 0.5mm and 2 mm respectively, and was directed to the proximal face of the phantom. Within the phantom, the beam's intensity attenuated exponentially with 1/e penetration depth of approximately $9\mu\text{m}$, which corresponds to a FWHM bandwidth of 90 MHz and deviates less than 7% from its maximum value over the 20 MHz bandwidth of interest. Thus, the optoacoustic source had the effective dimensions of 2mm x 0.5mm x $9\mu\text{m}$ and effectively emulated a point impulse-derivative source over a bandwidth of 20 MHz. The measured signal was integrated to obtain the impulse response, shown in Fig. 3a (dashed-red curve). The impulse response was Fourier transformed to obtain the frequency response, whose amplitude and phase are shown in Fig 3b and 3c. Figure 3d shows the amplitude of the impulse response in log scale. Figure 3 demonstrates a very good correspondence between the impulse and frequency responses obtained using method I (solid-blue curve) and method II (dashed-red curve).

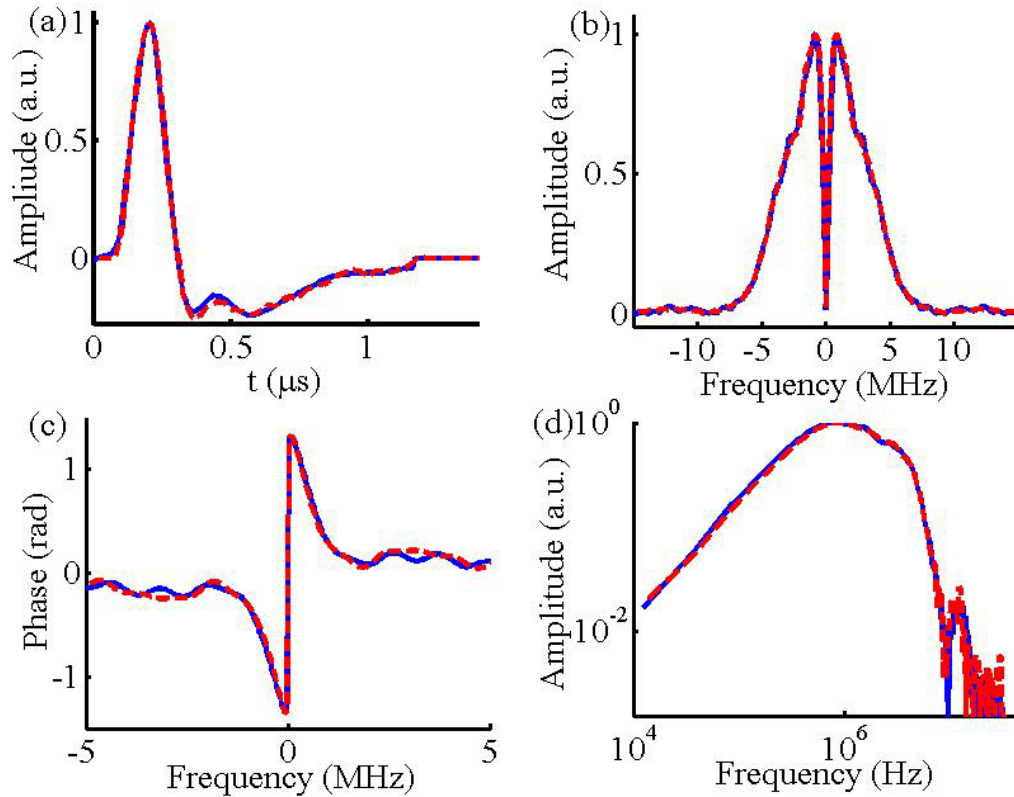


Fig.3 The (a) impulse response and (b,d) amplitude and (c) phase of the frequency response of the cylindrically focused acoustic detector obtained using method I (solid-blue curve) and method II (dashed-red curve).

3.3 Microspheres as optoacoustic point sources

In the third experiment, we measured an optoacoustic response from a physically small (point) source embedded in a clear agar phantom, as schematically shown in Fig. 2c. The phantom was prepared by molding a clear agar cylinder containing black-dyed polystyrene microspheres (Polysciences, Inc., Warrington, PA), each having a diameter of $10\ \mu\text{m}$, at an approximate concentration of 20 spheres per ml. A response from two different spheres was measured and analyzed. The results obtained for the two spheres are summarized in Fig. 4 (red solid curve, purple dashed curve) and compared to the results of method II (blue dotted curve). Figs. 4a and 4b show the measured response and its Fourier transform, respectively. The figures show a relatively good match between the three responses in both time and frequency domain. The main reason for the discrepancy between the different responses is that the location of the spheres within the agar phantom was random. Thus, the different responses relate to different locations in the plane of interest. In addition, slowly varying parasitic signals from the clear phantom and the tank boundary affected the results in the low frequency regime.

Since the responses in Fig 4a represent the derivative of the impulse response of the detector, they were integrated to obtain the impulse response. Figures 4c and 4d show the impulse and frequency responses of the detector, respectively. We note that the integration has accentuated the difference between the three responses, especially at low frequencies. Because the integration process amplifies the frequency response in the low frequencies, even minute discrepancies in the measured responses can lead to large deviations in the integrated response. In order to quantify the effect of the parasitic signal on the results, we performed the integration on sections of the signal that were outside the region of interest and did not contain the microsphere signal. The integrated parasitic signals had an average DC value of approximately 25% of the maximum response of the corresponding sphere. This indicates that the signals from the spheres in our setup were not sufficiently strong to measure the frequency response in the low frequency regime.

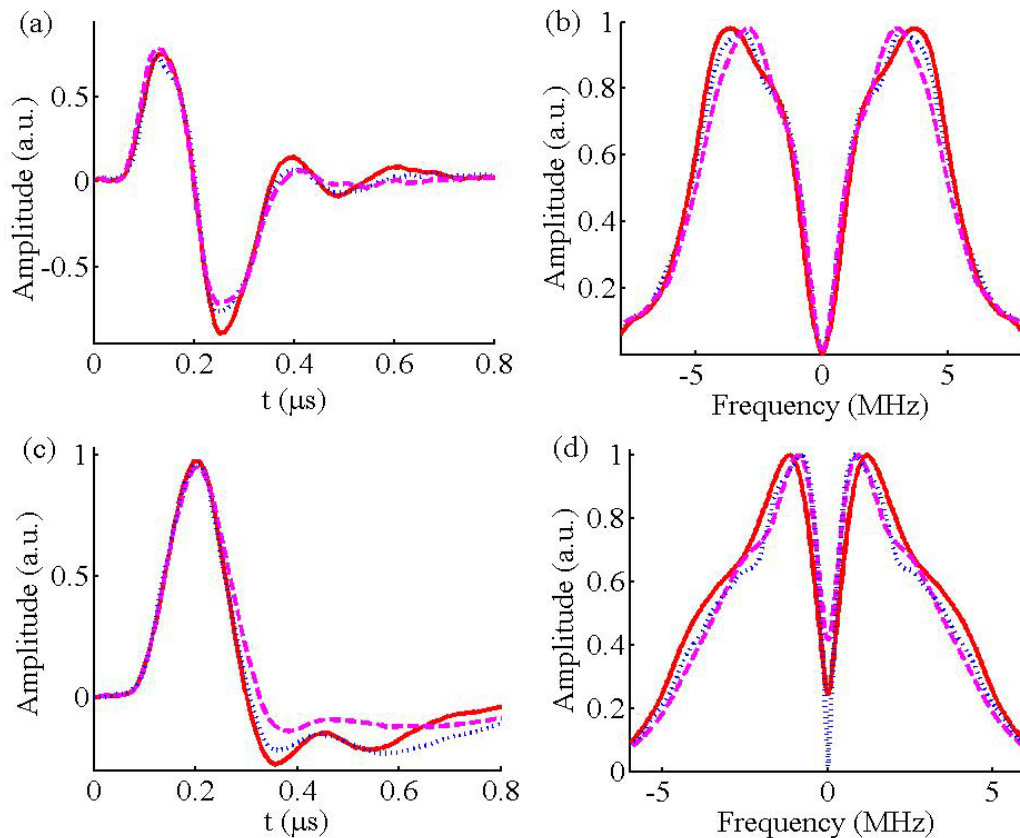


Fig.4 The responses obtained for two different microspheres, as depicted in Fig. 2c (solid-red curve and dashed-magenta curve) compared to the responses obtained for the geometry depicted in Fig. 2b (dotted-blue curve). The response of the transducer (a) in the time and (b) in the frequency domains. (c) The indefinite integral of the measured time-responses, which correspond to the impulse response of the detector, and (d) its Fourier transform, which corresponds to the frequency response of the detector.

4. CONCLUSIONS

In this paper we demonstrated two novel methods for measuring the frequency response of acoustic detectors to point sources. The main motivation for our calibration method is the emerging field of optoacoustic. Because in optoacoustic tomography the acoustic fields are generated within the imaged object, the sensitivity of the transducer should be measured for point sources located in the imaged region and not for plane waves. The difference between the two types of measurements becomes more apparent for both focused and flat large area detectors. Such detectors are commonly used in optoacoustic tomography because the large area leads to a higher sensitivity. In a focused-detector geometry, the fields originating from a point-impulse source at the focal point reach the transducer's surface at the same time, whereas a planar impulse wave reaches different parts of the surface at different times, thus limiting the bandwidth of the response. For the flat-surface transducer, the bandwidth becomes limited for point sources for the same reason.

In both the methods developed in this paper, the point sources were created by using the optoacoustic effect. This approach is ideal for calibrating acoustic detectors used in optoacoustic tomography systems because it enables measuring the response of the entire setup to an impulse point source located anywhere within the region imaged by the system. This allows one to simultaneously obtain a combined spectral and spatial sensitivity. In addition, the effects of

frequency-dependant acoustic attenuation and electric coupling of the transducer to the sampling system, which both affect the combined sensitivity of the setup, are readily taken into account in the measurement. Our method can also be used for open-circuit calibration of only the acoustic detector by modeling these effects and subtracting them from the measured results.

The main difficulty in utilizing the optoacoustic effect for acoustic-detector calibration is that the amplitude of optoacoustic sources is generally proportional to their dimensions, whereas their bandwidth is generally inversely proportional to their dimensions. This leads to the conclusion that in order for a localized optoacoustic source to have a large bandwidth, it must be extremely small, and consequentially weak. However, if the signal is too weak, it might be obscured by parasitic sources in the setup. This difficulty is particularly challenging in the low-frequency regime, where the signal from such small sources is even weaker.

We showed that in the case of rectangular sources, a different tradeoff between source dimensions and bandwidth may be obtained, which allows achieving wideband signals from large sources. We analyzed the response of such sources both analytically and numerically for different detector geometries. Based on our analysis, we developed two frequency-response-measurement techniques using large volume slab phantoms. In method I, the corresponding optoacoustic signal approximated an impulse function, whereas in method II it approximated a derivate of an impulse function. We demonstrated these two methods experimentally to measure to frequency response of a spherically focused transducer and obtained an excellent correspondence between the two measured spectra.

We compared our two methods to an ideal optoacoustic point source created by illuminating a dark microsphere. The frequency response was measured for two spheres with different locations. The obtained frequency responses showed a relatively good correspondence in the high frequencies to the one obtained using the slab phantoms. However, in the low-frequency regime, all three frequency responses exhibited different behaviors. The main reason for these differences is low-frequency parasitic signals, which accompanied the signals from the microspheres and were amplified by the integration process. This effect poses a technical difficulty to using microspheres for acoustic-sensor calibration. Nonetheless, it can still be successfully used for high-frequency calibrations, or in setups in which parasitic signals are minimized.

REFERENCES

- [1] MacLean W.R., "Absolute Measurement of Sound Without a Primary Standard", *J. Acoust. Soc. Amer.* 12, 140-146 (1940).
- [2] Bobber R. J., "C reciprocity parameter," *J. Acoust. Soc. Amer.* 39, 680-687 (1966).
- [3] Ludwig G. and Brendel K., "Calibration of Hydrophones Based on Reciprocity and Time Delay Spectrometry," *IEEE Trans. Ultrason. Ferroelec. Freq.* 35, 168-174 (1988)
- [4] Harris G. R. and Gammell P., "sensitivity measurements of piezoelectric polymer hydrophones from 0.2-2 MHz using broadband-pulse technique", *J. Acoust. Soc. Amer.* 105, 725-731 (1998).
- [5] Bacon D. R., "Primary Calibration of Ultrasonic Hydrophones Using Optical Interferometry," *IEEE Trans. Ultrason. Ferroelec. Freq.* 35, 152-161 (1988).
- [6] Koch C. and Molkenstruck W., "Primary calibration of hydrophones with extended frequency range 1 to 10 MHz using optical interferometry," *IEEE Trans. Ultrason. Ferroelec. Freq.* 46, 1303-1314 (1999).
- [7] Smith R. A. and Bacon D. R., "a multiple-frequency hydrophone calibration technique," *J. Acoust. Soc. Am.* 87, 2231-2243 (1990).
- [8] Kruger R. A., Liu P., Fang Y. R., Appledorn C. R., "Photoacoustic ultrasound (PAUS)--reconstruction tomography," *Med Phys.* 22, 1605-1609 (1995).
- [9] Wang X., Pang Y., Xie G. Ku, X., Stoica G., and Wang L. H. V., "Noninvasive laser-induced photoacoustic tomography for structural and functional in vivo imaging of the brain," *Nat. Biotechnol.* 21, 803-806 (2003).
- [10] Rosenthal A., Razansky D., and Ntziachristos V., "Fast semi-analytical model-based acoustic inversion for quantitative optoacoustic tomography", *IEEE Trans. Med. Imaging* 29, 1275 - 1285 (2010).
- [11] Razansky D., Distel M., Vinegoni C., Ma R., Perrimon R., Köster R. W., and Ntziachristos V., "Multi-spectral optoacoustic tomography of deep-seated fluorescent proteins in-vivo", *Nature Photonics* 3(7), 412 - 417 (2009).

- [12] Razansky D., Vinegoni C., and Ntziachristos V., "Multispectral photoacoustic imaging of fluorochromes in small animals", *Opt. Lett.* 32(19), 2891-2893 (2007).
- [13] Ma R., Taruttis A., Ntziachristos V., and Razansky D., "Multispectral optoacoustic tomography (MSOT) scanner for whole-body small animal imaging," *Optics Express* 17(24), 1414-21426 (2009).
- [14] de la Zerda A., Zavaleta C., Keren S., Vaithilingam S., Bodapati S., Liu Z., Levi J., Ma T., Oralkan O., Cheng Z., Chen X., Dai H., Khuri-Yakub B. T., Gambhir S. S., "Photoacoustic Molecular Imaging in Living Mice Utilizing Targeted Carbon Nanotubes", *Nat. Nano.* 3, 557-562 (2008).
- [15] Beard P. C., Perennes F., and Mills T. N., "Transduction mechanisms of the Fabry Perot polymer film sensing concept for wideband ultrasound detection," *IEEE Trans. Ultrason. Ferroelectr. Freq. Control* 46, 1575-1582 (1999).
- [16] Gamelin J., Aguirre A., Maurudis A., Huang F., Castillo D., Wang L. V., and Zhu Q., "curved array photoacoustic tomographic system for small animal imaging," *J. Biomedical Opt.* 13, 024007 (2008).
- [17] Conjusteau A., Ermilov S. A., Su R., Brecht H. P., Fronheiser M. P., and Oraevsky A. A., "Characterization of optoacoustic transducers through the analysis of angular dependent frequency response," *Proc. of SPIE Photons Plus Ultrasound: Imaging and Sensing* 7177, 71770U, (2009).
- [18] Cox B. T., Kara S., Arridge S. R., and Beard P. C., "k-space propagation models for acoustically heterogeneous media: application to biomedical photoacoustics," *The Journal of the Acoustical Society of America* 121, 3453-3464 (2007).
- [19] Ma R., Taruttis A., Ntziachristos V., and Razansky D., "Multispectral optoacoustic tomography (MSOT) scanner for whole-body small animal imaging," *Opt. Express* 17, 21414-21426 (2009).